PHYSICAL REVIEW B **79**, 245114 (2009)

Insulator to correlated metal transition in $V_{1-x}Mo_xO_2$

K. L. Holman,[1] T. M. McQueen,[1] A. J. Williams,[1] T. Klimczuk,[2,3] P. W. Stephens,[4] H. W. Zandbergen,[5] Q. Xu,[5]
F. Ronning,[2] and R. J. Cava[1]
[1]*Department of Chemistry, Princeton University, Princeton, New Jersey 08544, USA*
[2]*Los Alamos National Laboratory, Los Alamos, New Mexico 87545, USA*
[3]*Faculty of Applied Physics and Mathematics, Gdansk University of Technology, Narutowicza 11/12, 80-952 Gdansk, Poland*
[4]*Department of Physics and Astronomy, Stony Brook University, Stony Brook, New York 11794, USA*
[5]*Department of Nanoscience, National Centre for HREM, Delft Institute of Technology, 2628 CJ Delft, The Netherlands*
(Received 26 March 2009; published 15 June 2009)

Although many materials display the transition from insulating to metallic behavior on doping, only a few, such as VO_2, have the right combination of crystal structure and physical properties to serve as model systems. Here we report the electronic and structural characteristics of the insulator to metal transition in $V_{1-x}Mo_xO_2$, which we have studied over the range $0.0 \leq x \leq 0.50$ through characterization of the electrical resistivity, magnetic susceptibility, specific heat, and average- and short-range crystal structures. We find that metal-metal pairing exists in small domains in the doped metallic phases and an unexpected phenomenology for the crossover between a Curie-Weiss insulating regime and an intermediate mass metallic regime. An electronic phase diagram is presented.

DOI: 10.1103/PhysRevB.79.245114 PACS number(s): 71.30.+h, 71.10.Hf, 61.50.Ks, 75.20.Hr

I. INTRODUCTION

Materials that should be metallic conductors by simple electron counting and yet are electrical insulators have been of interest for decades as embodiments of strong electron-electron and electron-lattice interactions in solids.[1–3] Among the most iconic of such materials is VO_2, a compound whose Rutile crystal structure is based on chains of edge-sharing VO_6 octahedra. VO_2 undergoes a metal to insulator transition on cooling through 340 K, accompanied by a structural transition from tetragonal to monoclinic symmetry characterized by the formation of V-V pairs along the chains, tilted at an angle to the chain axis.[4–6] The V-V pairs are a classical example of a Peierls distortion,[7] with the V t_{2g} orbitals in the chain directions split into doubly occupied and empty states, localizing the $3d^1$ electrons on neighboring vanadium ions to form nonmagnetic spin singlets. This transition in VO_2 was first addressed theoretically in the 1970's, with arguments both for and against a pure Peierls picture for the origin of the insulator even at that early stage.[5,8–12] The issue is whether or not the structural distortion in the monoclinic phase is sufficient to completely separate the energies of the occupied chain-axis t_{2g} orbitals and those of empty t_{2g} orbitals aligned along other directions to create an insulator. The current understanding of VO_2 is that both the Peierls state, in which electrons on neighboring sites form localized spin singlets through the metal-metal pairing, and the Mott-Hubbard state, in which Coulombic repulsion between electrons attempting to occupy the same site introduces an energy gap, are needed to explain the insulating phase (e.g., Refs. 8 and 13–21).

Here we report the electronic and magnetic characteristics of the doping-induced insulator to metal transition in $V_{1-x}Mo_xO_2$. MoO_2 is nonmagnetic and isostructural with monoclinic VO_2 at room temperature and is metallic, with one extra electron per metal site.[22–24] We find that the electron doping of VO_2 through partial Mo substitution first results in the formation of Curie-Weiss magnetic states; the doped system is insulating at low temperatures at compositions where these magnetic states are largest in proportion. The Curie-Weiss states then partially delocalize on continued doping to form an intermediate mass metal with substantial magnetic character that evolves in an unexpected fashion with electron count. Diffraction evidence reveals that short-range ordered metal-metal pairs are present even in metallic $V_{1-x}Mo_xO_2$, implying that the Peierls state and spin singlets still exist locally even though the material is metallic. The results appear to be consistent with the Mott-Peierls scenario for VO_2, but determining how they fit in detail into developing models for the electronic properties of Rutile phases and metal-insulator transitions in general will require further study.

II. EXPERIMENTAL

Polycrystalline $V_{1-x}Mo_xO_2$ samples were synthesized for $0 \leq x \leq 0.50$ by standard solid-state techniques. High-purity VO_2, V_2O_3, V_2O_5, Mo, and MoO_2 starting materials were thoroughly ground together in the appropriate stoichiometric amounts, pressed into pellets, and sealed in evacuated quartz tubes. The tubes were slowly heated to 1150 °C and then held there for 10 days. The crystals employed for resistivity measurements in the metallic composition regime grew within the as-made pellets during the synthesis. The compositions of these crystals were confirmed by energy dispersive x-ray fluorescence analysis through comparison to polycrystalline standards, and their quality was confirmed by x-ray diffraction. The crystallographic unit-cell parameters at room temperature for all materials were determined by least-squares fits to laboratory x-ray powder diffraction peak positions, employing a Bruker D8 diffractometer with Cu $K\alpha$ radiation with a graphite diffracted beam monochromator. Quantitative structural refinement was performed for representative compositions using synchrotron powder x-ray diffraction data, collected at 300 K at the National Synchrotron Light Source at Brookhaven National Laboratory on beamline X16C. Rietveld refinements of the diffraction data were completed using TOPAS 2.1 (laboratory data) and GSAS[25,26] (synchrotron data). Electron-diffraction studies were performed with a CM200, and nanodiffraction with a beam diameter of about 5 nm with a CM300UT, both equipped with field-emission gun. Temperature-dependent magnetization measurements were performed in a Quantum Design Physical Property Measurement System (PPMS) system from 5 to 350 K; curves of M vs H were linear for all materials up to the 1 T measurement field employed, allowing the susceptibilities to be calculated from M/H, where M is the measured magnetization and H is the applied field. Temperature-dependent resistivity measurements were made between 2 and 370 K on bars cut from as-synthesized pellets, or along the c axis for single crystals for the metallic compositions, in the quantum design PPMS using the standard four-probe method. Heat-capacity data was obtained using a standard semiadiabatic heat-pulse technique in the quantum design PPMS on bars cut from as-made polycrystalline pellets or on powders pressed with Ag.

III. RESULTS

The overall structural behavior of the $V_{1-x}Mo_xO_2$ solid solution for $0.0\leq\times\leq0.5$ is reflected in the room-temperature crystallographic cell parameters [Fig. 1(a)]. A change from monoclinic to tetragonal symmetry marks the insulator to metal (I-M) transition near $V_{0.96}Mo_{0.04}O_2$ at room temperature. Although the variation in cell dimension perpendicular to the chains (a) in the tetragonal phase displays highly linear behavior as a function of Mo content, the c-axis cell parameter, which defines the unit cell along the chain direction, shows a broad maximum near $V_{0.8}Mo_{0.2}O_2$. The c lattice constant for MoO_2 at room temperature is smaller[22] than that of VO_2, so an overall decrease in cell parameter along the chain is expected for the $V_{1-x}Mo_xO_2$ series, but an initial increase followed by a decrease is unexpected. This behavior reflects subtle changes in the internal crystal structure and electronic properties of the system, described further below.

The c/a ratio in low-dimensional materials is often a useful probe of the response of the electronic system to doping. Figure 1(b) shows a comparison of the c/a ratios at room temperature in the tetragonal phases of metallic $V_{1-x}Mo_xO_2$ and insulating $V_{1-x}Nb_xO_2$.[27–29] Nb and Mo are neighbors in the periodic table, and their ions are very similar in size, and thus the dramatic difference in behavior for the two solid solutions is a reflection of the addition of the electron in the $V_{1-x}Mo_xO_2$ series compared to $V_{1-x}Nb_xO_2$. While the chain-perpendicular a axes grow by very similar amounts, 2.5–2.6 %, on going from $x=0.05$ to $x=0.50$ for the two systems, the chain parallel c axes behave very differently, with c in the Nb series increasing by 6% on going from $x=0.05$ to $x=0.50$ and c in the Mo series changing by very little. Therefore it can be inferred that the electron doping in the Mo series impacts the M-M pairing along the chains quite differently than does the Nb substitution, which adds no electrons to the system. Surprisingly, the differences in the chain perpendicular direction, where the lowest energy unfilled t_{2g} orbitals are found in VO_2 in current models, are relatively minor. Further insight into the M-M paring in the $V_{1-x}Mo_xO_2$ series is obtained from the crystal structure studies described below.

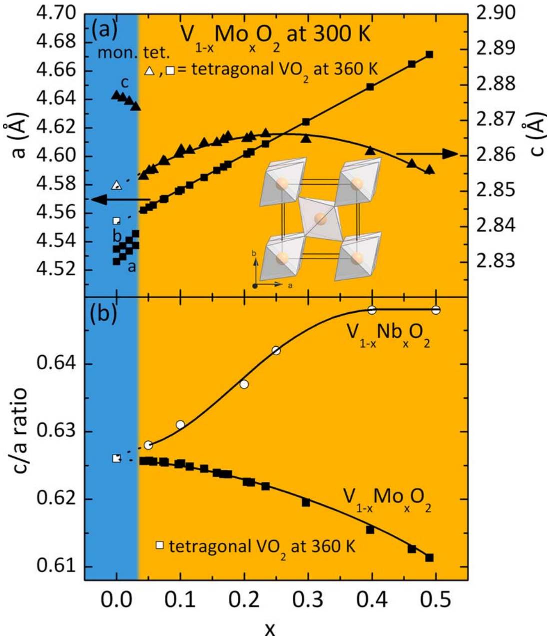

FIG. 1. (Color online) (a) Unit-cell parameters at 298 K for $V_{1-x}Mo_xO_2$ for $0\leq x\leq0.5$. For comparison, the monoclinic cell for low x has been transformed into the comparable tetragonal form, in which $\boldsymbol{a}_{\text{mon}}\approx2\boldsymbol{c}_{\text{tet}}$, $b_{\text{mon}}\approx a_{\text{tetr}}$, $\boldsymbol{c}_{\text{mon}}\approx\boldsymbol{b}_{\text{tetr}}-\boldsymbol{c}_{\text{tetr}}$. The cell parameters for pure VO_2 in the tetragonal phase at 360 K are also shown. Inset: the unit cell of tetragonal, high temperature VO_2; the VO_6 octahedra are emphasized in the polyhedral rendering. The chain direction is along the crystallographic c axis, and a is perpendicular to the chains. (b) The composition dependence of the c/a ratios for $V_{1-x}Mo_xO_2$ and $V_{1-x}Nb_xO_2$ show dramatically different behavior.

The temperature-dependent resistivities measured on polycrystalline samples (Fig. 2) show sharp increases on cooling through the metal to insulator (M-I) transitions, which are suppressed to lower temperatures as Mo doping increases, consistent with previous reports.[30,31] The M-I transition decreases in temperature and in magnitude with increasing x until a fully metallic state exists to low temperatures for $x>0.20$ (inset Fig. 2). A diffuse, weak resistive transition indicative of some remnant carrier localization is seen for compositions near $x=0.25$; for $x>0.25$, monotonic metallic behavior is observed.

The temperature-dependent magnetic susceptibilities (Fig. 3) are a more quantitative indication of the evolution of the $V_{1-x}Mo_xO_2$ electronic system with doping. Figure 3(a) shows the susceptibilities through the M-I transition at lower x, and [Fig. 3(b)] the susceptibilities for $x>0.20$, in the fully metallic regime. The data are consistent with earlier measurements for $x<0.20$, which were made to minimum temperatures of 77 K.[30] Pure VO_2 displays a very sharp drop in susceptibility to a low, temperature independent value below the M-I transition at 340 K [Fig. 3(a)], due to the gapping of

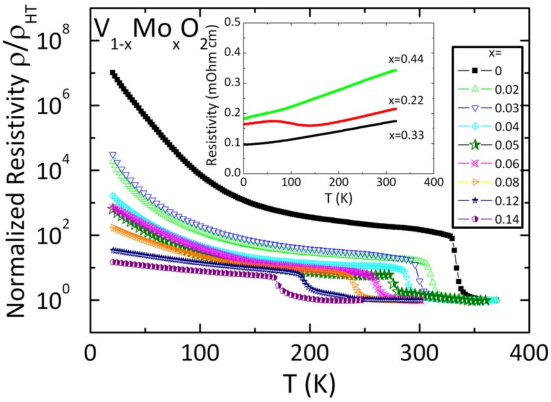

FIG. 2. (Color online) Normalized temperature-dependent resistivities for polycrystalline samples of $V_{1-x}Mo_xO_2$ $(0 \leq x \leq 0.14)$. Inset: temperature-dependent resistivities of single crystals of $V_{1-x}Mo_xO_2$ in the metallic composition regime, measured along the c axis.

the Fermi surface and the formation of spin singlets at the M-I transition. The M-I transition temperatures decrease with increasing x, and the sharp transition broadens in temperature for $x=0.18$, the highest composition for which insulating behavior is present at low temperatures.

The magnetic susceptibilities become smoothly varying with temperature for the $V_{1-x}Mo_xO_2$ metallic compositions, $x \geq 0.20$ [Fig. 3(b)]. A broad decrease in susceptibility is seen on cooling through 150–100 K in the metallic phases, which becomes washed out for $x \geq 0.35$ in part due to a decrease in the high-temperature susceptibility. The susceptibility at 250 K [χ_{250}, inset, Fig. 3(b)] shows a sharp increase at $x=0.07$, marking the I-M transition, but, in the metallic phase itself, χ_{250} decreases smoothly with increasing Mo content. This would not ordinarily be observed for a system where electrons are introduced into an insulator; rather, the electronic density of states and therefore the temperature independent susceptibility should increase with increasing doping.

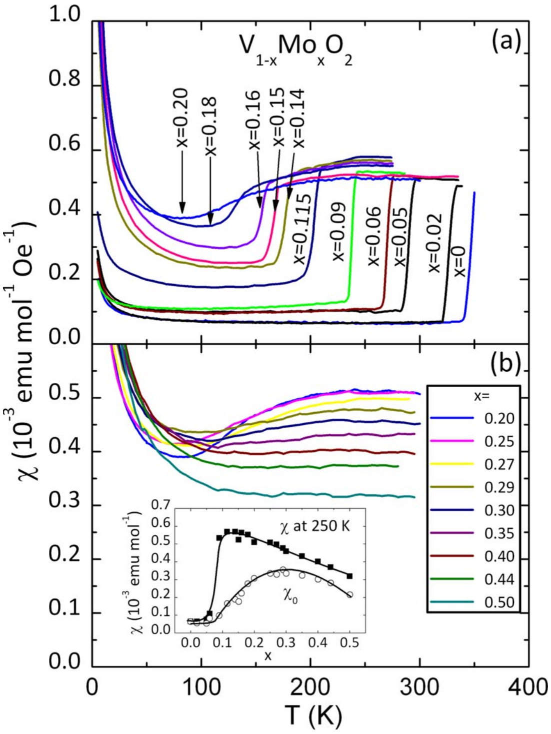

FIG. 3. (Color online) Temperature-dependent magnetic susceptibilities for $V_{1-x}Mo_xO_2$ (a) for $0 \leq x \leq 0.2$ and (b) for $0.2 \leq x \leq 0.5$. The metal-insulator transition temperature is marked by a sudden decrease in susceptibility. Inset (b), χ at 250 K increases sharply as the I-M transition is crossed on Mo doping, then slowly decreases in the metallic phase between $x=0.25$ and $x=0.50$. The temperature independent part of the low-temperature magnetic susceptibility, χ_0, determined from the fits (Fig. 4) is also shown.

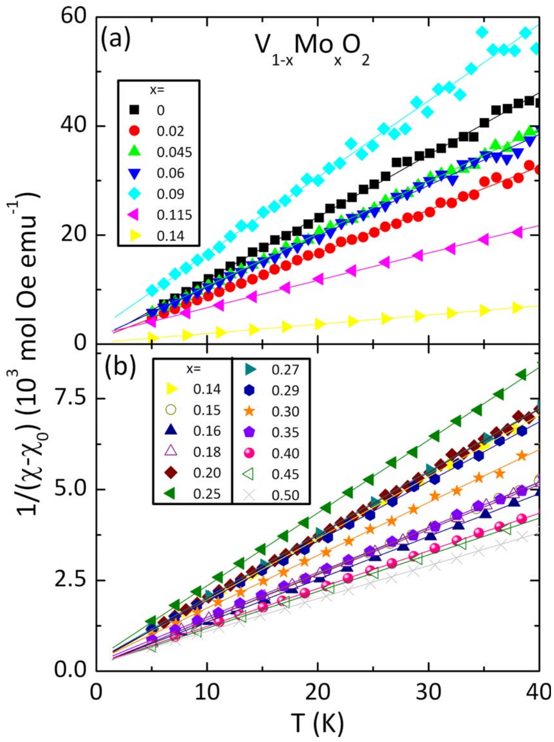

FIG. 4. (Color online) The low-temperature susceptibility data presented as $1/(\chi\text{-}\chi_0)$ versus T, with linear fits to the Curie-Weiss law from 5–40 K shown. (a) for $0 \leq x \leq 0.14$ and (b) for $0.14 \leq x \leq 0.5$.

A Curie-Weiss contribution to the susceptibilities is present at low temperatures for all $V_{1-x}Mo_xO_2$ compositions [Figs. 3(a) and 3(b)]. The low-temperature "Curie tail" is very small in pure VO_2 and the low-doping region ($x < 0.09$). It then systematically increases until it represents a major contribution to the susceptibility even for the compositions that are fully metallic to the lowest temperatures. We performed quantitative analysis of this data through fits of the susceptibility below 40 K to the Curie-Weiss law $\chi = C/(T+\theta_w)+\chi_0$, where C is the Curie constant, θ_w the Weiss temperature, and χ_0 the temperature independent part of the low-temperature susceptibility. The results of these fits are plotted as $1/(\chi\text{-}\chi_0)$ vs T in Figs. 4(a) and 4(b). Because the Mo ion does not have a local magnetic moment, the changes in the magnetic states on Mo doping are a reflection of the intrinsic behavior of the electron-doped VO_2 system (in the presence of disorder from the doped Mo). The doping introduces Curie-Weiss moments in $V_{1-x}Mo_xO_2$. The Weiss temperatures θ_w are antiferromagnetic and small, within a few

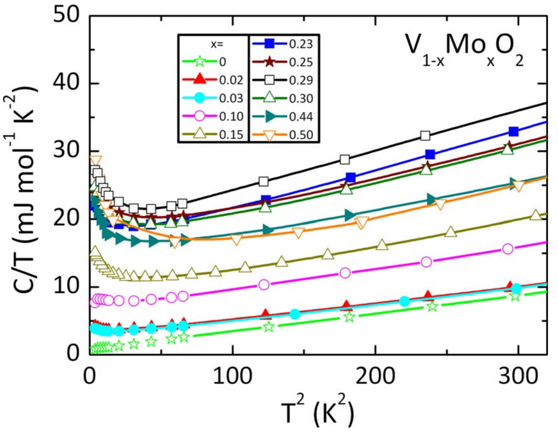

FIG. 5. (Color online) The low-temperature heat capacity for selected compositions in $V_{1-x}Mo_xO_2$, plotted as C_p/T vs T^2 to emphasize the $C_p = \gamma T + \beta T^3$ behavior. Lines are from the linear fits to the data at temperatures above the lowest temperature upturns.

Kelvin of zero for all compositions, and indicate very weak interactions between the magnetic species present. The composition dependence of χ_0 [inset Fig. 3(b)] shows a broad maximum near $x = 0.3$.

The low-temperature specific heats for the $V_{1-x}Mo_xO_2$ system are shown in Fig. 5. With the exception of the lowest temperatures for some compositions, the specific heat behaves as $C_p = \gamma T + \beta T^3$. Fits to the linear portions of C_p/T vs T^2 for temperatures below 18 K allow estimates for the electronic (γ) and lattice (β) contributions to the specific heat to be made. The β values yield Debye temperatures in the range of 470–630 K. γ increases dramatically with Mo doping, from approximately 1 mJ/mol K^2 for pure VO_2 to a maximum value of about 16 mJ/mol K^2 at $V_{0.75}Mo_{0.25}O_2$. It then decreases, to about 10 mJ/mol K^2 by $V_{0.50}Mo_{0.50}O_2$, where the curvature observed in the C_p/T vs T^2 behavior makes a good estimation of γ difficult. The observed composition dependence of γ is consistent with the composition-dependent trend in χ_0. The low temperature upturns in the specific heat seen in Fig. 5 correlate with the magnitudes of the Curie susceptibilities, and are characteristic of Schottky anomalies arising from fluctuations of the magnetic moments, the reason for the larger upturn for $V_{0.50}Mo_{0.50}O_2$, is not known.

Figure 6 shows the x dependence in $V_{1-x}Mo_xO_2$ of the electronic contribution to the specific heat (γ) and the effective moment per formula unit (p_{eff}) obtained from the low-temperature Curie-Weiss fits. A dramatic maximum in p_{eff} per formula unit is seen near 15% Mo doping, followed by a clear minimum and then a smooth increase with increasing x. The maximum in p_{eff} occurs just below the doping level where the system becomes fully metallic to low temperatures. At the same time, γ displays a broad maximum occurring in the composition region where the lowest p_{eff} is found in the metallic phase, and χ_0 is largest, at 25–30 % molybdenum doping. Comparison of γ to χ_0 allows an estimate of the Wilson ratio,[32,33] which is approximately 1.7 and independent of composition in the metallic phase. This indicates the presence of spin enhanced paramagnetism at low temperatures in the metallic regime. We conclude from these observations that metallic $V_{1-x}Mo_xO_2$ is a correlated electron system, as has been argued for the high-temperature metallic phase of VO_2.[21,34]

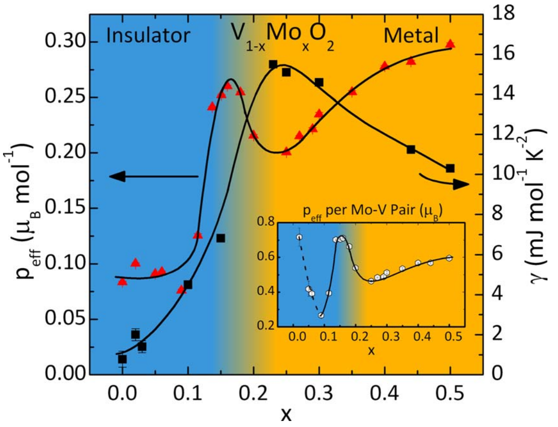

FIG. 6. (Color online) The effective moment per formula unit (p_{eff}) and the coefficient of electronic specific heat (γ), as a function of molybdenum doping in $V_{1-x}Mo_xO_2$. The comparison highlights the development of the Curie-Weiss moments on doping and then their decrease corresponding to the composition where the electronic specific heat is largest. Inset: The effective moment per $V_{\text{Mo-V}_{\text{pair}}}$ ($p_{\mathrm{eff}}^{\mathrm{pair}}$) as a function of composition.

A small fraction of crystallographic defects is always present in these phases, even for VO_2 itself. These defects in VO_2 give rise to a very weak Curie-Weiss contribution to the susceptibility at low temperatures [Fig. 3(a)]. These localized magnetic defects have been observed by EPR in pure VO_2 (Ref. 35) and attributed to the fact that one spin $\frac{1}{2}$ moment is released per defect-broken V-V singlet pair. The data in $V_{1-x}Mo_xO_2$ show that electron doping introduces Curie-Weiss moments that increase abruptly above an apparent threshold of $x \sim 0.1$ (Fig. 6). Our electron-diffraction studies showed the presence of no short range or long range Mo-V ordering in $V_{1-x}Mo_xO_2$, and therefore that there is a random distribution of Mo and V in the metal sites. This allows the fraction of Mo-V, Mo-Mo, and V-V pairs to be calculated statistically as a function of composition. If a local-moment picture holds for the whole $V_{1-x}Mo_xO_2$ solid solution, then each Mo-V pair created on doping would break a spin singlet and release one spin $\frac{1}{2}$ moment, while the V-V and Mo-Mo pairs would be nonmagnetic. The inset to Fig. 6 presents the observed effective moment per V-Mo pair as a function of composition. Mo doping first decreases the defect-induced moment per V-Mo pair at low x, but then, for compositions above $x = 0.1$, where the doping-induced magnetic species dominate the low-temperature susceptibility, the effective moment per V-Mo pair sharply increases, peaking near $0.7\mu_B$ at the composition $V_{0.85}Mo_{0.15}O_2$. It then drops sharply to a lower but still significant value, and then increases weakly with composition for higher x. If broken singlets were the origin of the observed Curie Weiss moments in $V_{1-x}Mo_xO_2$, then p_{eff} per Mo-V pair would be independent of composition and equal to the spin $\frac{1}{2}$ value of $1.7\mu_B$. This is clearly not the case, indicating that a local picture, attributing the observed moments in $V_{1-x}Mo_xO_2$ to broken singlets is not valid.

In the current picture for the M-I transition in VO_2, the formation and tilting of the V-V pairs lifts the t_{2g} orbital degeneracy and splits and narrows the t_{2g} electronic bands pointing along the chain direction. The result is that the two-electron σ bonding band of a V-V dimer is filled entirely (with one electron per V) and the antibonding band is empty and pushed to much higher energy. The remaining, broader t_{2g}, π, and δ electronic bands lie just above the filled σ band. These empty states overlap the filled σ states in energy in all electronic models that do not include electronic correlations, and therefore, it is argued, Mott physics is necessary to yield the insulator. A doping-induced I-M transition would consequently arise primarily due to the introduction of electrons into the broader π and δ bands, with only a secondary influence on the σ states associated with the V-V pairs. To test whether the crystal structures of the doped phases provide any insight into this possibility, we have determined, by high-resolution synchrotron x-ray powder diffraction, the room-temperature crystal structures for $V_{1-x}Mo_xO_2$ in the metallic composition regime. We find that the average crystal structures of the metallic $V_{1-x}Mo_xO_2$ phases are rigorously tetragonal ($P4_2/mnm$), with no peak splitting that would suggest a lowering of symmetry. We also find, however, that the ideal tetragonal Rutile crystal structure, which has a uniform, single M-M distance along the chains, and therefore no M-M pairing, does not provide a satisfactory agreement between observed and calculated x-ray diffraction intensities for the metallic phases. We find instead that the metal ions are displaced significantly from the ideal Rutile sites $[2a(0,0,0)]$ along the chain directions. This displacement [to positions $4e(0,0,z)$] splits each ideal Rutile metal site into two sites displaced $\pm z$ along the chain directions, with each of the displaced sites half-occupied statistically in the average structure. The metal displacement from the ideal site is highly significant for the whole series, with a refined value of, for example, $z=0.0282(8)$ for $V_{0.7}Mo_{0.3}O_2$-defined to better than 35 standard deviations as different from the ideal Rutile structure position of $z=0.0$. Figure 7 shows how well the structural model fits the observed data for $V_{0.7}Mo_{0.3}O_2$. The structural data for the $V_{1-x}Mo_xO_2$ series are presented in Table I. Structural models for which the metals were allowed to move off the chain axis, i.e., to metal positions of the type (x,x,z) or $(x,0,z)$, such as would be the case if the pairs were tilted away from the chain axis, did not result in improvements in the fits.

Figure 8(a) shows the intrapair and interpair M-M separation determined from the crystal structure refinements as a function of Mo doping in $V_{1-x}Mo_xO_2$. Differences in the composition dependencies of these separations are the underlying cause of the broad peak in the composition dependence of the c axis in the tetragonal phase seen in Fig. 1. Due to the disorder, our average structure refinements do not provide sufficiently detailed local information to say whether the M-M pairs are tilted away from the chain direction or not, but conclusions about the pairing can none-the-less be drawn by looking at the evolution of the pair separation in the $V_{1-x}Mo_xO_2$ series, presented in Fig. 8(b). The end members of the $V_{1-x}Mo_xO_2$ solid solution are both monoclinic, and both show pairing and tilting, even though VO_2 is insulating and MoO_2 is metallic. MoO_2 has shorter interpair M-M distances than VO_2 does, and thus the addition of one electron per site has not weakened the strength of the pairing. Metallic $V_{1-x}Mo_xO_2$, on the other hand, shows interesting behavior. On first addition of electrons to induce metallicity, e.g., at $V_{0.95}Mo_{0.05}O_2$, the pairs are substantially weakened—the short M-M separation has clearly lengthened, independent of whether the pairs are tilted locally or not (because the projection of the separation in $V_{0.95}Mo_{0.05}O_2$ along c is much longer than the actual V-V separation in VO_2, and, if tilted locally, then the separation would be even larger). Surprisingly, the pairs then strengthen again as more electrons are added in the solid solution, approaching what is seen in MoO_2. Thus our data show that the M-M bonding along the chain is increasing in strength as electrons are doped into $V_{1-x}Mo_xO_2$ after an initial weakening when metallicity is first induced. How this behavior fits into a detailed electronic analysis of pairing in VO_2 and MoO_2 will be of interest in future research.

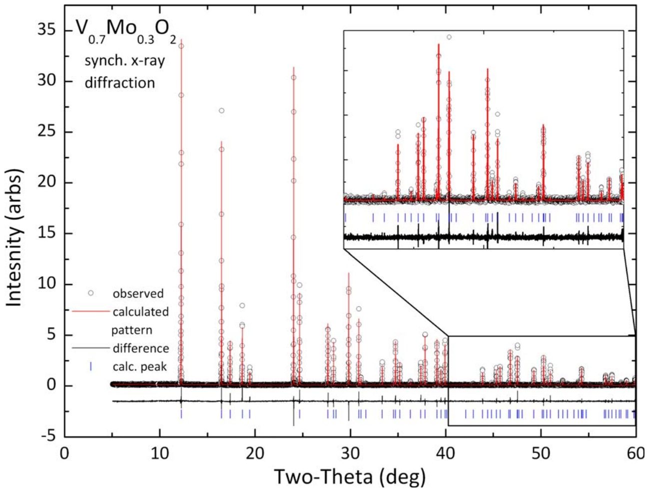

FIG. 7. (Color online) Room temperature synchrotron powder x-ray diffraction pattern of $V_{0.70}Mo_{0.30}O_2$, a representative composition in the metallic composition regime. The points are the observed intensities, and the solid line is the fit to the structural model in the tetragonal phase that includes displacements of the V/Mo ions from their ideal positions to form metal-metal pairs. The line at the bottom of the plot, the difference between the model and the fit, shows the excellent agreement. Inset: detail of the high-angle region showing the excellent quality of the fit.

The metal ion displacements are the signature of the Peierls distortion, and thus the crystal structure refinements indicate unambiguously that M-M pairs are present in metallic $V_{1-x}Mo_xO_2$. Unlike the case for insulating VO_2, however, the statistical occupancy shows that the M-M pairs are only short-range ordered in the doped metallic phases. To obtain a more local picture of the structure of the metallic phases, nanoscale electron diffraction was performed at room temperature on compositions within the metallic regime. With a relatively large incident electron beam (diameter >100 nm), the diffraction patterns e.g., for $V_{0.5}Mo_{0.5}O_2$ [Fig. 9(a)] reveal the presence of weak superlattice reflections at positions in the reciprocal space of the tetragonal phase that indicate the presence of small twin domains in the material. Scanning crystallites with a beam focused to cover an area of about 5 nm correspondingly showed two sets of superlattice reflections, in different spatial regions; Fig. 9(b) displays primarily

TABLE I. Crystal structure parameters for the tetragonal symmetry compositions of $V_{1-x}Mo_xO_2$ at 300 K, determined by refinement of synchrotron x-ray powder diffraction data. Space group $P4_2/mnm$. Unit-cell parameters a and c (in Å), V and Mo in position 4e, which is statistically occupied with 0.5 atom per site, O in position 4f, atomic positions in fractional cell coordinates, isotropic thermal parameters Uiso in Å^2, standard deviations in parentheses. χ^2 is the measure of the goodness of fit.

x	a(Å)	c(Å)	Metal 4e Occ.=0.5r $(0,0,z)$: z=	100*Uiso	O 4$f(x,x,0)$: x=	100*Uiso	χ^2
0.05	4.564113(10)	2.854644(8)	0.0153(16)	1.438(18)	0.29900(28)	1.69(4)	1.404
0.10	4.575081(10)	2.859941(8)	0.0221(11)	1.309(20)	0.29893(28)	1.25(4)	1.414
0.15	4.587521(11)	2.863239(8)	0.0151(14)	1.743(20)	0.29731(27)	1.56(4)	1.467
0.20	4.599248(10)	2.864916(7)	0.0277(6)	1.712(16)	0.29697(24)	1.86(4)	1.502
0.30	4.624448(14)	2.865083(10)	0.0282(8)	1.457(20)	0.29434(33)	1.43(5)	1.431
0.35	4.635750(10)	2.863865(7)	0.0239(8)	1.334(17)	0.29297(30)	1.21(4)	1.564
0.40	4.649020(10)	2.861941(7)	0.0341(4)	1.042(15)	0.29370(31)	1.26(4)	1.495
0.50	4.679790(13)	2.853946(8)	0.0371(4)	1.634(14)	0.29312(26)	1.62(4)	1.714

one of the sets. The diffraction patterns observed with the beam size of greater than 100 nm are therefore a superposition of diffraction patterns from several very small regions: the true local symmetry is observed only in the very small region whose diffraction pattern is seen in Fig. 9(b). The positions and intensities of the observed superlattice reflections are consistent with those expected for a monoclinic VO_2-like structure. The true local structure of the metallic $V_{1-x}Mo_xO_2$ phases is therefore monoclinic, with a domain size on the order of 10 nm. VO_2-like M-M pairs are still present in the doped metallic $V_{1-x}Mo_xO_2$ phase, with the same out of phase relationship between pairs on neighboring chains, but the coherence of the pairs has been broken on a very short length scale. Averaging the very small monoclinic domains over their different orientations yields the tetragonal average structure characterized in the powder x-ray diffraction experiment. These nanometer-scale monoclinic domains may be the correlated metallic regions recently observed in VO_2 just above its I-M transition.[36]

Our proposed general phase diagram for the $V_{1-x}Mo_xO_2$ system is presented in Fig. 10. The M-I transition temperature of 340 K in VO_2 decreases linearly with Mo concentration, consistent with previous reports.[30] This linear decrease

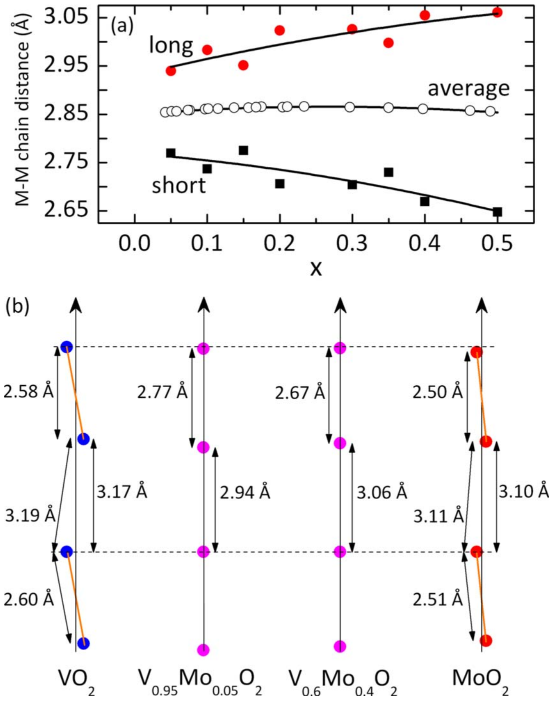

FIG. 8. (Color online) (a) The composition-dependent evolution of the M-M pair separations within the metallic phase in $V_{1-x}Mo_xO_2$ at room temperature. (b) Comparison of the M-M pair separations and c-axis projections for VO_2 and MoO_2, and the average pair separations for several compositions in the $V_{1-x}Mo_xO_2$ series. The drawing is to scale in absolute units, with dotted lines to guide the eye.

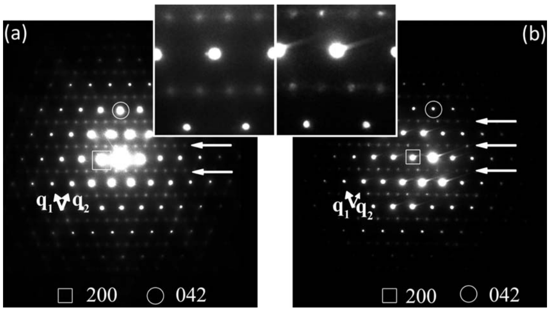

FIG. 9. (a). Typical electron-diffraction pattern ([02–1] diffraction zone) of $V_{0.5}Mo_{0.5}O_2$ at room temperature, taken with an incident beam probing a relatively large area (>100 nm). The strong peaks in the diffraction patterns are indexed using the basic tetragonal lattice of VO_2 ($a=b=4.68, c=2.85$); the positions of the superlattice reflections (marked by horizontal arrows) can be described with an additional vector q. There are two sets of superlattice reflections, with q's along $\frac{1}{2}(121)^*$ and $\frac{1}{2}(12-1)^*$. (b) The [02–1] diffraction zone recorded from a very small area (<10 nm): two sets of superlattice reflections are still seen, but with clearly different intensities, indicating that the symmetry of the material over short distances is monoclinic, not tetragonal. The insets show portions of the electron-diffraction patterns in detail.

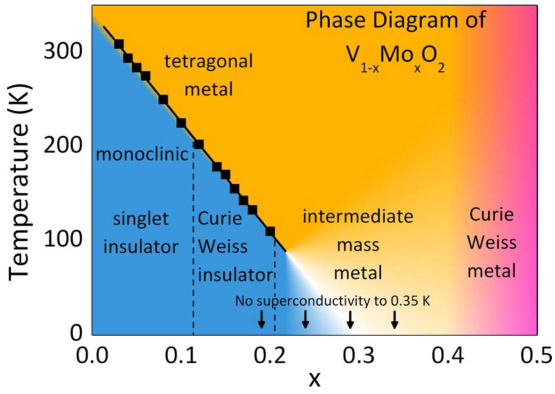

FIG. 10. (Color online) The proposed electronic phase diagram for $V_{1-x}Mo_xO_2$.

with doping is unusual and is thus far unexplained. For x greater than about 0.16, the once-sharp M-I transition broadens; and beyond $x=0.18$ can no longer be seen. The white area in the diagram corresponds to the region where the crossover from a Curie Weiss moment state to an intermediate mass state is observed. Four compositions in this composition region ($x=0.18$, 0.25, 0.30, and 0.35) were tested resistively for superconductivity and were found to be normal metals down to 0.35 K. At higher x, beginning at about 0.4, the decreases in γ and χ_0 and the corresponding increase in p_{eff} suggest a subtle crossover to a metal in which the electronic states give rise to dominantly Curie-Weiss rather than paramagnetic behavior.

IV. DISCUSSION AND CONCLUSIONS

The metallic state in $V_{1-x}Mo_xO_2$ occurs in the presence of the Peierls distortion, and thus that distortion alone is not sufficient to result in an insulating material even at low doping (i.e., $x=0.05$ at 300 K). The Peierls pairing is robust against the electron doping, though it does change in detail. The metallic state and the tetragonal symmetry crystal structure with no V-V pairing are intimately linked in undoped VO_2.[37] Our x ray and electron-diffraction studies of the metallic phase of $V_{1-x}Mo_xO_2$ show, however, that the apparent tetragonal symmetry in the doped case arises due to spatial averaging over very small domains, each with monoclinic symmetry. A short-range ordered Peierls state exists in the metallic phase of $V_{1-x}Mo_xO_2$, and thus the M-I transition in doped VO_2 (for compositions such as $V_{0.9}Mo_{0.1}O_2$) is not strictly analogous to that in undoped VO_2: for the doped phases, a transition from short range to long range ordered Peierls states must also play a role at the M-I transition.

In a local picture, the appearance of Curie-Weiss magnetism in $V_{1-x}Mo_xO_2$ would be attributed to broken spin singlets, with each Mo-V pair releasing a spin. This appears to be the case for insulating $V_{1-x}Nb_xO_2$, where the Nb dopant is 5+, $4d^0$ spin 0, and every doped Nb^{5+} quantitatively releases one localized spin 1 moment, as a V^{4+}-V^{4+} spin singlet pair becomes a V^{3+} $(3d^2,\text{spin } 1)$-Nb^{5+} pair.[10,27–29,38] Local moments observed in insulating Ga[39] and W[40] doped VO_2 have also been attributed to broken singlets. $V_{1-x}Mo_xO_2$, however, is much less straightforward, as the induced magnetic moment is not directly proportional to the Mo concentration and never reaches the local-moment spin $\frac{1}{2}$ value. Although this implies that the moments are itinerant in $V_{1-x}Mo_xO_2$, a sharp dividing line between localized and itinerant behavior on going from Nb to Mo dopants in VO_2 would be surprising.

The current study thus lends support to the Mott-Peierls scenario for the metal to insulator transition in VO_2, but at the same time raises questions about localized vs itinerant behavior when VO_2 is chemically doped to a metallic conductivity, and further about how the long- and short-range crystal structures observed reflect the underlying changes in the electronic states. Our results suggest that detailed studies of the local electronic and structural character of the system, such as through scanning tunnel microscope or optical characterization of the electronic and magnetic states on the nanometer length scale, and local structural probes to determine the character of the M-M pairs, would be of great interest in $V_{1-x}Mo_xO_2$. The issue of electronic and structural homogeneity on nanometer length scales is also likely to be of interest for other classical doped Mott or Peierls insulators.

ACKNOWLEDGMENTS

The work at Princeton was supported by the National Science Foundation under Grants No. NSF DMR02-13706 and No. DMR-0703095. The work at Los Alamos and the use of the National Synchrotron Light Source, Brookhaven National Laboratory, were supported by the U.S. DOE, BES (Brookhaven Grant No. DE-AC02-98CH10886). T.M.M. gratefully acknowledges support of the National Science Foundation Graduate Research Foundation. R.J.C. gratefully acknowledges discussions with A. Lichtenstein.

---

[1] N. F. Mott, *Metal Insulator Transitions* (Taylor and Francis, London, 1990).

[2] P. P. Edwards and C. N. R. Rao, *The Metallic and Non-metallic States of Matter* (Taylor and Francis, London, 1985).

[3] M. Imada, A. Fujimori, and Y. Tokura, Rev. Mod. Phys. **70**, 1039 (1998).

[4] F. J. Morin, Phys. Rev. Lett. **3**, 34 (1959).

[5] J. B. Goodenough, J. Solid State Chem. **3**, 490 (1971).

[6] C. N. Berglund and H. Guggenheim, Phys. Rev. **185**, 1022 (1969).

[7] R. E. Peierls, *Quantum Theory of Solids* (Clarendon, Oxford, 1955), p. 108.

[8] J. P. Goodenough and H. Y. P. Hong, Phys. Rev. B **8**, 1323 (1973).

[9] A. Zylbersztejn and N. F. Mott, Phys. Rev. B **11**, 4383 (1975).

[10] J. P. Pouget, H. Launios, T. M. Rice, P. Dernier, A. Gossard, G. Villeneuve, and P. Hagenmuller, Phys. Rev. B **10**, 1801 (1974).

[11] J. P. Pouget, H. Launois, J. P. D'Haenens, P. Merenda, and T. M.

Rice, Phys. Rev. Lett. **35**, 873 (1975).

[12] M. Gupta, A. J. Freeman, and D. E. Ellis, Phys. Rev. B **16**, 3338 (1977).

[13] S. Biermann, A. Poteryaev, A. I. Lichtenstein, and A. Georges, Phys. Rev. Lett. **94**, 026404 (2005).

[14] S. Shin, S. Suga, M. Taniguchi, M. Fujisawa, H. Kanzaki, A. Fujimori, H. Daimon, Y. Ueda, K. Kosuge, and S. Kachi, Phys. Rev. B **41**, 4993 (1990).

[15] A. Liebsch, H. Ishida, and G. Bihlmayer, Phys. Rev. B **71**, 085109 (2005).

[16] R. M. Wentzcovitch, W. W. Schulz, and P. B. Allen, Phys. Rev. Lett. **72**, 3389 (1994).

[17] M. W. Haverkort, Z. Hu, A. Tanaka, W. Reichelt, S. V. Streltsov, M. A. Korotin, V. I. Anisimov, H. H. Hsieh, H. J. Lin, C. T. Chen, D. I. Khomskii, and L. H. Tjeng, Phys. Rev. Lett. **95**, 196404 (2005).

[18] T. C. Koethe, Z. Hu, M. W. Haverkort, C. Schussler-Langeheine, F. Venturini, N. B. Brookes, O. Tjernberg, W. Reichelt, H. H. Hsieh, H.-J. Lin, C. T. Chen, and L. H. Tjeng, Phys. Rev. Lett. **97**, 116402 (2006).

[19] U. Schwingenschlögl and V. Eyert, Ann. Phys. **13**, 475 (2004).

[20] M. S. Laad, L. Craco, and E. Muller-Hartmann, Phys. Rev. B **73**, 195120 (2006).

[21] J. M. Tomczak, F. Aryasetiawan, and S. Biermann, Phys. Rev. B **78**, 115103 (2008).

[22] A. A. Bolzan, B. J. Kennedy, and C. J. Howard, Aust. J. Chem. **48**, 1473 (1995).

[23] A. Gulino, S. Parker, F. H. Jones, and R. G. Egdell, J. Chem. Soc., Faraday Trans. **92**, 2137 (1996).

[24] V. Eyert, R. Horny, K. H. Hock, and S. Horn, J. Phys.: Condens. Matter **12**, 4923 (2000).

[25] B. H. Toby, J. Appl. Crystallogr. **34**, 210 (2001).

[26] A. C. Larson and R. B. Von Dreele, Los Alamos National Laboratory Report No. LAUR 86-748, 2000 (unpublished).

[27] W. Rüdorff and J. Märklin, Z. Anorg. Allg. Chem. **334**, 142 (1964).

[28] G. Villeneuve, A. Bordet, A. Casalot, J. P. Pouget, H. Launois, and P. Lederer, J. Phys. Chem. Solids **33**, 1953 (1972).

[29] J. P. Pouget, P. Lederer, D. S. Schreiber, H. Launois, D. Wohlleben, A. Casalot, and G. Villeneuve, J. Phys. Chem. Solids **33**, 1961 (1972).

[30] T. Horlin, T. Niklewski, and M. Nygren, Mater. Res. Bull. **8**, 179 (1973).

[31] A. Prodan, V. Marinkovic, and M. Prosek, Mater. Res. Bull. **8**, 551 (1973).

[32] K. Wilson, Rev. Mod. Phys. **47**, 773 (1975).

[33] Z. Fisk, H. R. Ott, and G. Aeppli, Jpn. J. Appl. Phys. **26**, 1882 (1987).

[34] M. M. Qazilbash, K. S. Burch, D. Whisler, D. Shrekenhamer, B. G. Chae, H. T. Kim, and D. N. Basov, Phys. Rev. B **74**, 205118 (2006).

[35] J. Pietrzak, J. Kudynska, and Z. Kruczynski, Phys. Status Solidi A **67**, K175 (1981).

[36] M. M. Qazilbash, M. Brehm, B. G. Chae, P. C. Ho, G. O. Andreev, B.-J. Kim, S.-J. Yun, A. V. Balatsky, M. B. Maple, F. Keilmann, H.-T. Kim, and D. N. Basov, Science **318**, 1750 (2007).

[37] D. B. McWhan, M. Marezio, J. P. Remeika, and P. D. Dernier, Phys. Rev. B **10**, 490 (1974).

[38] P. Lederer, H. Launois, J. P. Pouget, A. Casalot, and G. Villeneuve, J. Phys. Chem. Solids **33**, 1969 (1972).

[39] W. Bruckner, H.-P. Bruckner, U. Gerlach, B. Thuss, and G. Foersterling, Phys. Status Solidi A **38**, K13 (1976).

[40] T. Horlin, T. Niklewski, and M. Nygren, Mater. Res. Bull. **7**, 1515 (1972).